Safety assessment of underground vehicles passing over highly resilient curved tracks in the presence of a broken rail

B. Suarez, P. Rodriguez, M. Vazquez and I. Fernandez

Vehicle-track interaction for a new resilient slab track designed to reduce noise and vibration levels was analysed, in order to assess the derailment risk on curved track when encountering a broken rail. Sensitivity of the rail support spacing, of the relative position of the rail breakage between two adjacent rail supports and of running speed were analysed for two different elasticities of the rail fastening system.In none of the cases analysed was an appreciable difference between either of the elastic systems observed. As was expected, the most unfavourable situations were those with greater rail support spacing and those with greater distance from the breakage to the nearest rail support, although in none of the simulations performed did a derailment occur when running over the broken rail. When varying the running speed, the most favourable condition was obtained for an intermediate speed, due to the superposition of two antagonistic effects.

Safety assessment of underground vehicles passing over highly resilient curved tracks in the presence of a broken rail

B. Suarez[1*], P. Rodriguez[1], M. Vázquez[2], I. Fernández[2]

[1] *Departamento de Ingeniería Mecánica y Fabricación. Universidad Politécnica de Madrid.*
ETSI Industriales (CITEF), C/ Jose Gutierrez Abascal, 2, ES-28006 Madrid, SPAIN
[2] *Metro de Madrid, S. A. C/ Cavanilles, 58, Madrid, SPAIN*

* Corresponding author: Berta Suarez, e-mail: citef-bsuarez@etsii.upm.es,
Postal address: ETSI Industriales (CITEF), C/Jose Gutierrez Abascal, 2, ES-28006 Madrid, SPAIN

Vehicle-track interaction for a new resilient slab track designed to reduce noise and vibration levels was analysed, in order to assess the derailment risk on curved track when encountering a broken rail. Sensitivity of the rail support spacing, of the relative position of the rail breakage between two adjacent rail supports and of running speed were analysed for two different elasticities of the rail fastening system.
In none of the cases analysed was an appreciable difference between either of the elastic systems observed. As was expected, the most unfavourable situations were those with greater rail support spacing and those with greater distance from the breakage to the nearest rail support, although in none of the simulations performed did a derailment occur when running over the broken rail. When varying the running speed, the most favourable condition was obtained for an intermediate speed, due to the superposition of two antagonistic effects.

Keywords: slab track, resilient track, curved track, block spacing, broken rail, derailment risk

Aims and scope

The demand for higher running speeds and payloads is worsening the problem of vibration propagation in railway lines. This effect can be mitigated by reducing the vertical stiffness of the rail supports, although this can derive in large vertical displacements, which could affect track stability. In addition, the combination of high track elasticity with a high running speed could increase the risk of derailment when running over a rail breakage.

Rail breakages are of great concern in long distance railway operations since they are one of the main causes of track-related derailment. In underground operations, however, this type of accident rarely occurs, due to the moderate running speeds used.

In order to ensure a good acoustic and vibratory behaviour of the track for the forthcoming extension plans of the Metro de Madrid network, this railway administration considered the possibility of installing a new track system involving high-elasticity rail supports. Although throughout its more than 90 years of history no derailments have occurred related to the passage of the wheels over a broken rail, prior to making a final decision, a preliminary study was performed in close collaboration with the Centro de Investigación en Tecnologías Ferroviarias (Railway Technologies Research Centre) of the Universidad Politecnica de Madrid (Madrid Polytechnic University). This study analysed how vehicle running safety can be affected by the installation of this new type of elastic track when a train runs over a broken rail.

In the 1995–1999 expansion plan, when heavier and faster vehicles were acquired (axle load of 15.5 tons and a running speed of 110 km/h), the standard Edilon independent block system (Embedded Block System – Standard Stiffness, EBS-SS) was installed for the new operating conditions. In further expansion plans, it was decided to install a track system with an even better performance in order to improve passenger comfort and reduce noise and vibration emissions. The behaviour of the new, more elastic system, called EBS-Medium Stiffness (EBS-MS), was installed in Metrosur and has given highly satisfactory results. After that, Edilon developed another even more elastic system called EBS-Low Stiffness (EBS-LS) for future projects.

In a previous piece of research, the dynamic behaviour of vehicle–slab track interaction on straight tracks in the presence of a broken rail (Figure 1) was analysed (1).

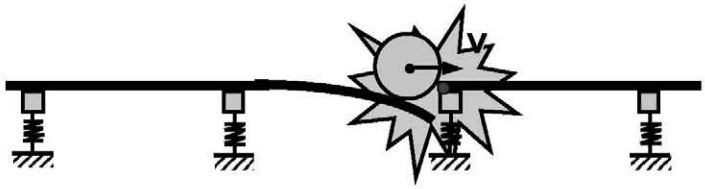

Figure 1 The problem of a broken rail

In this paper, the results of a further study concerning rail breakage on curved tracks are presented. In this new study, the effect of the rail support spacing, of the relative position of the rail breakage between two adjacent supports and of the running speed on a curved track were analysed. All these variations were carried out for two elastic properties of the track. For all these situations, it was assessed to what extent the train's derailment safety would be affected by a broken rail, and whether or not a possibility of derailment existed.

State of the art

In recent years, a lot of research has been conducted in the field of railway vehicle dynamics simulation, (2) and (3). In particular, a detailed study of vehicle–track interaction has been the focus of many researchers (4), (5), (6), (7), (8), (9), (10), (11), (12), (13) and (14). Nevertheless, little has been investigated in the field of broken rails and their influence on the vehicle's riding behaviour and safety, with the exception of the analytical work carried out by Eisenmann (15). Some interesting statistical results can also be found in references (16) and (17).

Apart from these works, a previous study concerning derailment risk related to rail breakages on straight track has been recently published by the same authors (1).

In the following paragraphs, some previous studies concerning the following topics are described:

- relation between rail breakage and derailments;
- rail impacts;
- highly resilient fixation systems and
- derailment criteria.

Relation between rail breakage and derailments

On tracks with continuous welded rail, the joints between rails are one of the weakest points of the track, with failures in welds being one of the causes of derailments on long-distance lines (16). These failures can be originated by track fatigue, by rail impacts or by the poor quality of some welds.

Some studies made in the United States (17) have found a strong correlation between the number of rail defects detected by visual inspection and the derailments produced by rail breakage.

Temperature variations affect the tensional state of the rails, which are compressed in summer and stressed in winter, with the critical values occasionally being exceeded. Breakages are more common in cold months, due to poor welding procedures during the summer, when not enough time is taken to reach the equilibrium temperature needed to obtain a correct weld (16). In addition, in ballasted tracks, tamping and ballast cleaning machines can magnify this problem, since tamping is not recommended in summer in order to avoid buckling problems, while in winter these works stress the rail when raising it and enlarge the cracks.

Rail impacts

Rail discontinuities can generate high impact forces between wheel and rail when the wheel passes over them (18). Although the dynamic phenomenon that takes place when a wheel runs over a rail breakage is not described in any publication, many publications deal with the impacts produced when running over a dipped rail joint. Although the impact produced when running over a rail breakage is stronger, some similarities can be found between these two types of rail singularities. Some features of the interaction between wheel and dipped rail joints are described below.

On encountering a discontinuity, the wheel descends and the rail raises (18). Due to its inertia, the wheel cannot follow the track defect, and a contact loss takes place, with a consequent reduction of the contact force. When the wheel contacts again with the rail, an impact takes place, and the contact force suddenly increases, producing a peak value. This peak force can be very high, especially at high speeds (19).

The dynamic loads produced by an impact in a dipped rail joint are made up of a short duration peak, P1, and a delayed peak, P2 (20). The former appears when the wheel batters the rail-end corner, and the latter is related to rail bending. Since it is related to a more resilient mode, the P2 peak has a smaller magnitude and a greater duration than P1.

Sensitivity studies made by Jeong have shown the great influence of the running speed and of the separation between both rail ends on the dynamic load related to the passage over a dipped rail joint (21), (20).

Highly resilient fixation systems

In tracks with stiff fixation systems, the vibrations transferred by the vehicle wheels can be transmitted to the surrounding terrain (3). This can be avoided by using more resilient fixations, making the transmission of vibrations towards the lower part of the track difficult. These more resilient fixations also allow a greater deflection of the rail, thereby distributing the vehicle load over considerably more ties.

Using super resilient fixations, with a dynamic stiffness of about 6 kN/mm, the wheel/rail resonance frequency can be reduced to 20 Hz (22). This is very effective for reducing noise and vibrations. Noise attenuation up to 20 dB(A) can be obtained together with an average vibration reduction of 20 dB in the 25 to 120 Hz frequency band. The installation of these systems could reduce the number of rail breakages as well as rolling contact fatigue.

One drawback is that an excessive reduction in stiffness can lead to greater stresses and deflections, the latter being high enough to affect track stability (22), (23). On some lines of the New York and Milan underground systems, a super resilient fixation system has been installed, in which resilient elements are preloaded up to 90 % of the wheel static load, in order to avoid an excessive deformation of the track. In this way, rail deflection remains within the acceptable limits.

Other similar products for metropolitan operations have been developed, with excellent vibroacoustic behaviour (23). A solution of highly resilient floating slab track, specially designed for high speeds and high axle loads, has been successfully installed in one of the sections of the high speed line of the Channel Tunnel, near London. Before its final installation on the line, preliminary designs showed that the reduction of the lateral and vertical track stiffness did not have any significant effect on safety and ride quality.

Some other considerations concerning the behaviour of highly resilient tracks can be found in (22), (23) and (24).

Derailment criteria

In this section, some derailment criteria used by different institutions are described (25). As will be seen, most of them use the ratio between wheel-rail lateral, Y, and vertical, Q, loads.

Nadal's criterion

According to this criterion, the wheel will not derail if:

$$\frac{Y}{Q} \leq \frac{tg\alpha - \mu}{1 + \mu \cdot tg\alpha}$$

Where α is the wheel flange angle and μ the wheel-rail friction coefficient. For the usual values of these parameters, the limit value falls between 0.8 and 1.2.

This criterion is appropriate for high angles of attack ($\approx$ 10 mrad), but conservative for small or negative ones. It considers that the wheel flange climbs the rail instantaneously once the limit value is surpassed, although field tests have shown that this value must be exceeded during a certain period of time.

Weinstock's criterion

This criterion establishes a limit value for the sum of the absolute values of the Y/Q quotient for the left and right wheels of the same wheelset:

$$\sum \left| \frac{Y}{Q} \right| \leq \frac{tg\alpha - \mu}{1 + \mu \cdot tg\alpha} + \mu$$

The value limit is the sum of the Nadal index limit of the wheel that tends to lift the rail, plus the friction coefficient in the other wheel. It is a less conservative criterion than Nadal's, giving better accuracy for small or negative angles of attack.

Duration based criterion

According to this criterion, for lateral thrusts below 50 ms, the limit value proposed by Nadal should be increased.

Wheel climb duration limit

This criterion, used by the AAR, fixes the wheel lift duration to 50 ms. The limit value applied to Y/Q for any wheel must be smaller or equal to 1, and the limit value applied to the sum of the absolute values of Y/Q for any wheelset must be smaller or equal to 1.5, during time periods greater than 50 ms.

Wheel climb distance criterion

According to this criterion, used by the FRA, a wheel climb distance of 5 feet should be considered for high speed tracks of class 6 or higher.

Wheel unload criterion

Since the previous criteria are useful for assessing wheel lift derailment risk, this criterion is more suitable for rollover derailment risk. According to this criterion (26), the vehicle will not derail when:

$$\frac{\Delta Q}{Q_0} \leq \frac{(-\mu^2)\,tg\alpha - 2\cdot\mu + 2\cdot\theta\cdot(+\mu\cdot tg\alpha)}{(+\mu^2)\,tg\alpha}$$

Where Q_0 is the wheel static load, α the wheel flange angle, μ the wheel-rail friction coefficient and θ the track superelevation angle. For a friction coefficient of 0.36 and a superelevation angle of 0.1 rad, the limit value is 0. 667.

Characteristics of the system analysed

Slab track

The highly resilient supports, which are the object of this study, are integrated into a slab track system. General features of slab track systems were described in a previous paper (1). Other useful references are (27), (28), (29), (30) and (31).

The slab track system installed in Metro de Madrid (Figure 2) uses two independent concrete blocks instead of sleepers (28), (29), (32), (33), (34), (35). Each block is jointed to a tray by an elastomeric compound, thus forming a prefabricated structure called an embedded block. The final slab track is constructed by pouring concrete underneath the embedded blocks until the concrete level reaches the height of the trays and forms the concrete slab. Finally, the rails are fixed on top of the embedded blocks. The spacing between two adjacent blocks is usually fixed to 1.0 m for straight tracks. On curved tracks, the block spacing may vary from 0.75 to 1.0 m, depending on the curve radius. The rails are clamped to the embedded blocks by means of standard fastening mechanisms. An elastic rail pad is introduced between the rail and the embedded block.

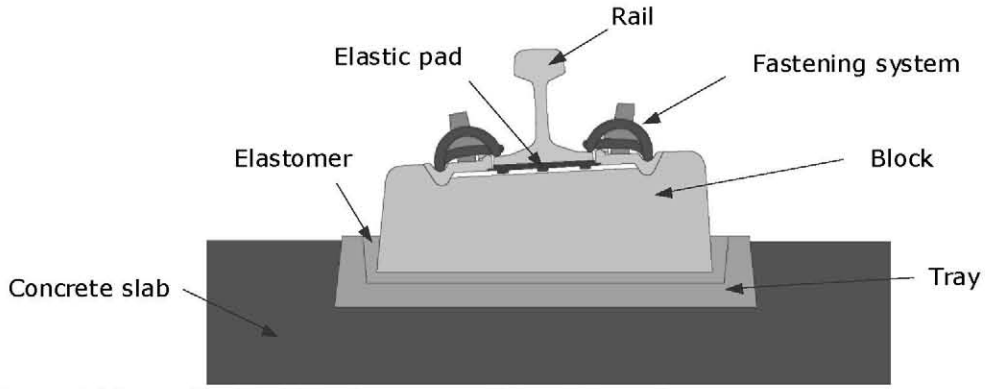

Figure 2 The embedded block system of the slab track

As previously stated, the purpose of this study was to compare the dynamic behaviour of the two elastic systems considered: EBS-MS and EBS-LS, the stiffness and damping properties of which (32) are shown in Table 1.

Parameter (slab track)	**SS System**	**MS System**	**LS System**
Block spacing, *l*	1.0 m		
Vertical stiffness, *k*	60.0 kN/mm	15.5 kN/mm	7.0 kN/mm
Vertical damping, *d*	29.5 kNs/mm	4.54 kNs/mm	4.1 kNs/mm

Table 1 Elastic properties of the EBS-SS, EBS-MS and EBS-LS systems

Rolling stock

Since this study is mainly focused on wheel-rail interaction, where impacts may appear when encountering a broken rail, the most active component of the vehicle is the wheelset (21), which represents the un-sprung mass. For this reason, the study was reduced to a single type of vehicle. The vehicle chosen for this study was a 6000 series metropolitan car from Metro de Madrid's rolling stock (Figure 3).

Figure 3 6000 series vehicle

Reference model

In this work, both FEM and MBS modelling techniques were integrated. In this way, a complex three-dimensional MBS vehicle model was combined with an FEM elastic track model (Figure 4). The wheel–rail contact forces are crucial for studying derailment risk and therefore have to be considered in the modelling. The track's elastic

behaviour could not be disregarded either, as a broken rail was to be modelled. The modelling techniques used allow for modelling curved tracks, which are usually not considered in conventional models with elastic track. An extended state-of-the-art review of the dynamic modelling of the track and its interaction with the vehicle can be found in references (2), (3), (36) and (37).

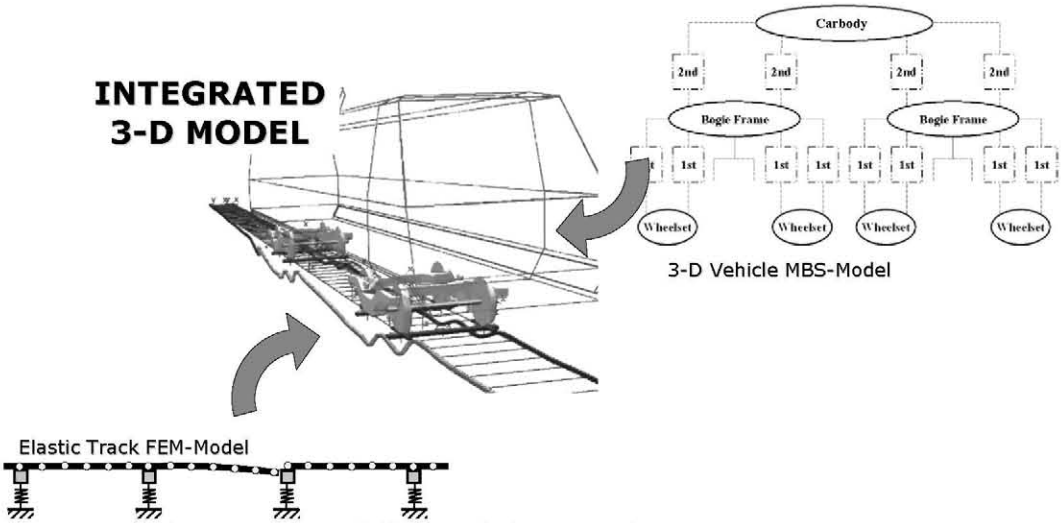

Figure 4 The integrated modelling technique used

Vehicle model

Railway vehicle models have two special characteristics that differentiate them from other generic multibody systems: the longitudinal guidance and the wheel-rail contact, which involves great forces transmitted through a small surface (37). In this study, the SIMPACK commercial program was used, which allows simulating multibody systems with these features.

The main bodies of the vehicle (car-body, bolsters, bogie frames and wheelsets) were modelled as rigid bodies connected to each other by means of springs and dampers that characterise the primary and secondary suspensions. The mechanical properties of the car-body include the structure, the interior layout, the exterior and interior equipment and the payload, and those of the bogie the structure of the bogie frame, the brake system, the motor-gearbox group and half of the suspensions.

According to the results obtained in the previous study on straight track (1), a full load condition was considered for the vehicle model, as this is the most unfavourable situation.

The whole vehicle model was extensively described in reference (38).

Slab track model

The track analysed in the study was Metro de Madrid's modern slab track that was described above (33). The equivalent slab track model can be characterised by elastic steel rails (UIC 54) and embedded blocks. The stiffness and damping parameters used for describing the track's behaviour (Table 1) include the elastic properties of the fastening system, the elastic rail pad, the embedded block, and the elastomer located between the blocks and trays (Figure 2).

The elastic rails were modelled in the ANSYS FEM-program and later introduced in the SIMPACK MBS-program. The discrete embedded blocks were modelled in SIMPACK by means of force elements.

For this study, the most unfavourable layout in Metro de Madrid's network was used, with the minimum possible curve radius, R = 300 m, and the maximum allowed superelevation, h = 150 mm.

Selecting the breakage position

In order to find the most unfavourable point of the track where the rail breakage should be located, a simulation was performed of the vehicle running at 75 km/h on a rigid curve with a 300 m radius, 150 mm superelevation and no breakage. When analysing running safety, it was observed that the most critical values were obtained both at the start and end points of the section with constant radius. Figure 5 shows the Nadal index obtained for the outer wheels.

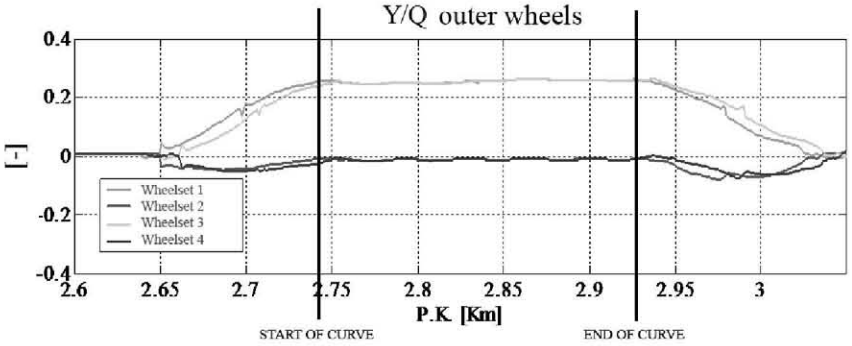

Figure 5 Nadal's index on the curved track

Following these results, the breakage point was located just on entry to the curve in order to shorten the duration of the simulations. A track with an initial straight section of 15 m was modelled, so that the train could initially be on a straight track, followed by a transition section of 100 m and a final curved section with a 300 m constant radius and 40 m in length (Figure 6). The overall track length was 155 m, with the breakage point located 115 m from the starting point.

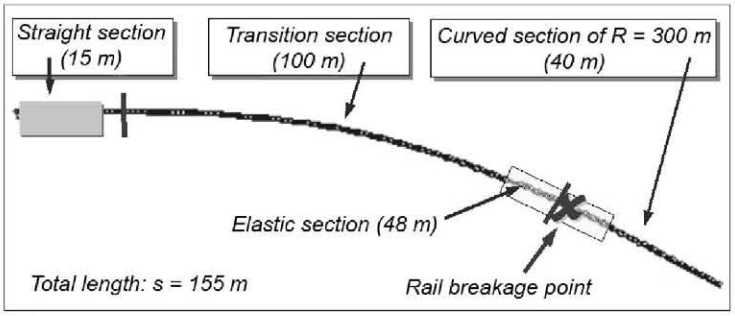

Figure 6 Setup of the curved track model

Modelling in ANSYS

Three rails were modelled in ANSYS by means of Rayleigh-Timoshenko one-dimensional beams: a 155 m unbroken rail, and the first and second fragments of the broken rail, measuring 115 and 40 m, respectively.

Due to the limitations of SIMPACK regarding the total number of nodes, the elasticity of the initial and final sections of the track was disregarded, since the zone of interest lies in the proximities of the breakage. It was estimated that the zone of influence for the study of the breakage was about 24 m from both ends of the breakage, resulting in a 48 m elastic section in the unbroken rail, and a 24 m elastic section in both fragments of the broken rail (see Table 2).

Elastic body	**Length [m]**	**No. modes**	**Max. frequency**
Unbroken rail	155	80	1270 Hz
1st rigid section	91		
Elastic section	48		
2nd rigid section	16		
Broken rail (before breakage)	115	80	4436 Hz
Rigid section	91		
Elastic section	24		
Broken rail (after breakage)	40	80	4431 Hz
Elastic section	24		
Rigid section	16		
Node spacing in elastic sections	0.1	-	-
Node spacing in rigid sections	1	-	-

Table 2 Characteristics of elastic rail models

A 0.1 m node spacing was used in the elastic sections, with bending degrees of freedom in the vertical plane, and a 1.0 m node spacing in the rigid sections, with no degrees of freedom. Lateral displacements were disregarded, their being outside the scope of this study.

The position and direction of each node depends on the exact geometry of the track, both in the transition and in the constant radius sections. These data were obtained from an auxiliary SIMPACK model with a rigid track exactly like the one being modelled in ANSYS. In this way, the vertical degree of freedom allowed in the nodes of the elastic sections is normal to the plane of the track, thereby considering the rotation with respect to the horizontal plane due to the superelevation.

The mass and stiffness matrices were calculated in ANSYS, along with the first 80 eigenfrequencies (see Table 2) and their corresponding mode shapes. The number of modes considered in the calculation was high enough to take into account the dynamic responses of the rails up to 1200 Hz. According to (36), this is the adequate frequency range for studying impact phenomena related to discontinuities in the track.

Modelling in SIMPACK

The data calculated in ANSYS was then imported into the SIMPACK vehicle model by means of an intermediate module called FEMBS. SIMPACK uses the modal superposition technique (2) to calculate the deformation of the elastic bodies used to model the left and right rails. The structural damping of the rails was considered to be negligible and was not taken into account.

In order to facilitate a variation of the block spacing, the embedded blocks were modelled directly in SIMPACK by means of force elements with the elastic properties

shown in Table 1. The distance between the force elements was 1.0 m, equal to the block spacing.

As previously indicated, the broken rail was modelled by two independent rails. By separating these rails, a discontinuity between the two rails was obtained to simulate the broken rail. The relative position of the discontinuity between two adjacent blocks was adjusted by appropriately positioning the force elements. Figure 7 shows the configuration that was considered in the final simulation models, with the train coming in from the left. As can be seen, the breakage is located just before one of the embedded blocks.

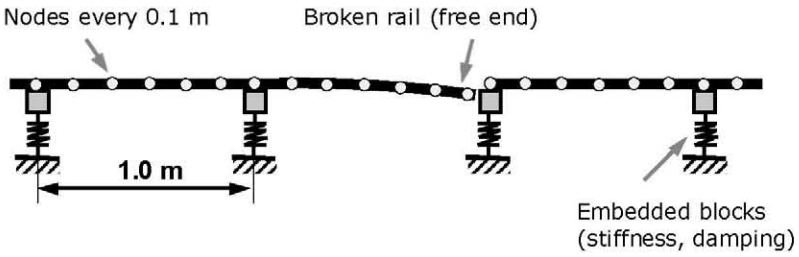

Figure 7 Position of the gap that represents the broken rail

However, both the block spacing and the breakage location were also changed in further simulations, as will be shown further on.

Vehicle-Track interaction model

The calculation of wheel-rail interaction was performed with the SIMPACK Wheel/Rail module. The contact condition between the wheel and the rail was characterised by a Hertz contact spring with zero stiffness in traction, so as to allow contact loss. The creepage forces were calculated by SIMPACK using the FASTSIM algorithm, which applies the simplified Kalker's theory.

Wheel-rail contact forces calculated by SIMPACK can only be directly applied on rigid bodies. Thus, in order to transfer wheel-rail normal forces to the elastic bodies used to model the rails, a set of auxiliary bodies had to be defined, as described below.

First, a floating auxiliary body was defined per wheelset. Floating bodies rest on two vertical springs and also move along the track, each following one wheelset. Loads from both wheels of each wheelset are transferred to the corresponding floating body through Hertzian springs. After that, a set of moved markers was defined on each elastic body, in particular one marker per wheelset. Like the floating bodies, each moved marker moves along its own elastic body, following a specific wheelset.

When no rails were broken, the left spring of the floating body was attached to a moved marker defined on the left rail, while the right spring was attached to a moved marker defined on the right rail (Figure 8). The moved markers used to attach these springs were those which follow the same wheelset as the floating body. In this way, the wheel normal force can be transferred through the vertical springs to the corresponding elastic bodies.

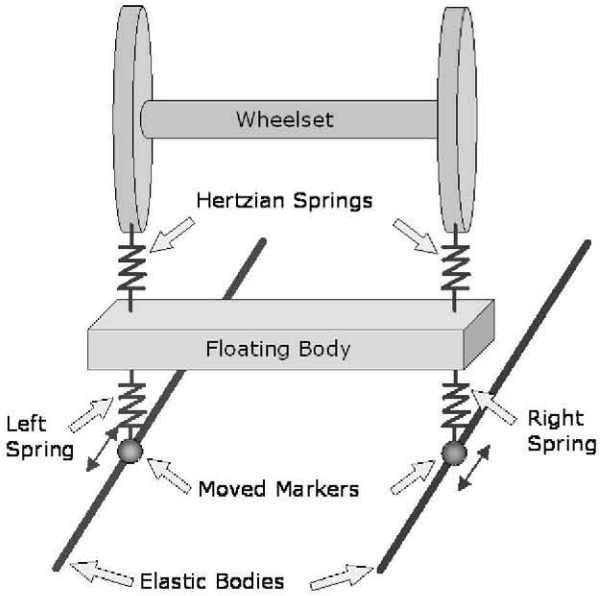

Figure 8 Floating body and moved markers for standard elastic track

As the broken rail was modelled by two elastic bodies, a third vertical spring had to be added when the rail was broken, so that the floating body could be simultaneously connected with the three elastic bodies used to model the track (Figure 9).

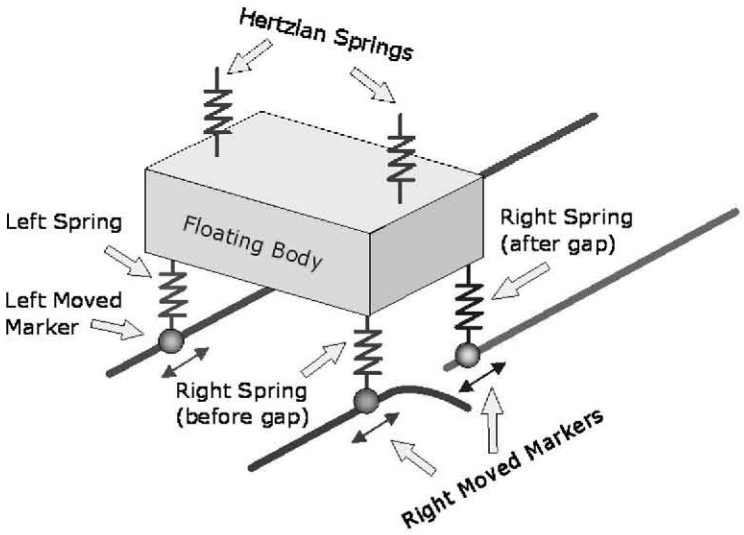

Figure 9 Floating body and moved markers for models with a broken rail (right rail)

The presence of the broken rail added a further difficulty to the model, since the moved markers moved along the track in a continuous way, not taking into account any discontinuity. To overcome this drawback, the wheel load had to be transferred only to that segment of the broken rail over which the wheelset was placed. Load transfer to the other segment had to be avoided. To achieve this result, a special force element had to be programmed to allow the passing of the wheels from the rail before the gap to the rail after the gap. This force element provides a zero value when the wheelset is not directly placed over the elastic body on which the spring is fixed, the force expression being:

$$F^i = \begin{cases} k_z \cdot \Delta z + c_z \cdot v_z & ,\text{if}(x_0^i < x < x_{end}^i) \\ 0 \quad \text{otherwise} \end{cases}$$

where i is the index of the aforementioned elastic body, and x_0^i and x_{end}^i are, respectively, its first and last node longitudinal coordinates.

Once the model was completed, the static equilibrium position for the unmoving vehicle was calculated in order to obtain the static deflection of the rails under the vehicle's weight. Figure 10 shows a snapshot of the final SIMPACK model used in the simulations. The deflection of the elastic track under the vehicle's weight was represented after applying a scaling factor.

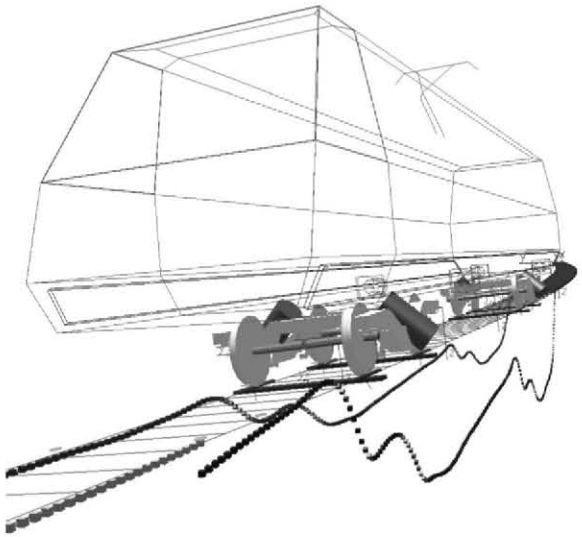

Figure 10 The final MBS-model.

Simulations and results

As previously stated, a reference model was defined as a starting point for the simulations. In this reference model the vehicle ran at 80 km/h over a curved track with a 300 m radius and 150 mm superelevation, 1 m embedded blocks spacing, and a breakage located just before one of the embedded blocks. This reference speed was calculated as the maximum speed at which that curve could be negotiated so that the uncompensated lateral acceleration would fall below 0.65 m/s^2, which is the allowed limit in Metro de Madrid's network. The maximum axle load of 15.5 tons was also used, as this is the most unfavourable situation.

The effect of the rail on which the breakage is located, inner or outer, of the embedded block spacing, of the relative position of the rail breakage between two adjacent supports and of the running speed were analysed for the two elastic properties of the track, EBS MS and EBS LS.

The vehicle's derailment risk was estimated by evaluating the Nadal and wheel unload criteria. To complete the evaluation of the vehicle's running behaviour, the vertical displacement of the free end of the broken rail was also calculated.

In order to make the comparison of the results easier, only the maximum values were displayed and compared with one another. These maximum values were divided by the limit value of each index, set at 0.67 for the wheel unload index and at 0.8 for Nadal's index so that the results could be expressed as a percentage of its limit value.

As the maximum values for derailment risk using Nadal's index are only reached during a very short interval of time, Miyamoto (39) stated the importance of taking into account the time length during which this index is larger than its limit value. He also suggested that the average value over time should be used as a new criterion for safety evaluation. Sharing this idea, Ishida and Matsuo (40) suggested applying a 2 m window sliding mean, thus ignoring instantaneously high values. This value is also recommended by the UIC-518 leaflet (41), where the 99.85 percentile is also used instead of the actual maximum value. Although no mention was found in the literature regarding statistical processing for the wheel unload index, the authors considered applying the same mathematical processing to this index.

Following the indications of the UIC-518 leaflet, a Butterworth low-pass filter with a 20 Hz cut-off frequency was initially applied to the signals, followed by the mathematical processing indicated above. Although the characteristic peaks observed in the signals when passing over the rail breakage are smoothed when applying this mathematical processing, its use was considered appropriate, since the limit values used in the derailment criteria were also established for signals subjected to the complete mathematical processing recommended by the UIC-518 leaflet.

The results obtained for all the cases analysed are shown in the following paragraphs.

Effect of the rail on which the breakage is located

Cases Analysed

In order to determine the most unfavourable location for the rail breakage, in the inner or outer rail of the curve, two simulations were performed with the same embedded block system (EBS MS), but with the breakage located in a different rail. The simulated cases were named Mi and Mo (Table 3). The first letter, M, refers to the embedded block system used (MS), while the second one identifies the broken rail (i=inner, o=outer).

Case	**Embedded block system (stiffness and damping)**	**Breakage location**
Mi	KMS, dMS	Inner rail
Mo		Outer rail

Table 3 Cases used to analyse the effect of the rail in which the breakage is located

Comparative results

The maximum values of the vertical deflection of the free end, the wheel unload index and Nadal's index are shown in Figure 11, for both cases, Mi and Mo.

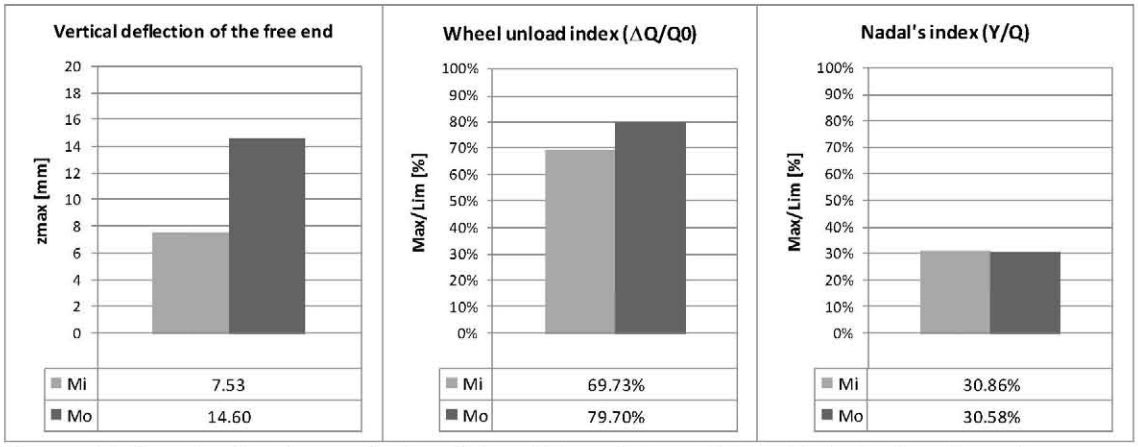

Figure 11 Results for the analysis of the effect of the rail in which the breakage is located

As can be seen, the rail deflection is greater when the broken rail is the outer one (Mo), almost doubling the deflection obtained for the Mi case. This is due to the fact that when running over a curve the outer rail is loaded, while the inner one is unloaded.

The wheel unload index is also 10 % greater when the outer rail is broken (Mo), although it remains below its limit value. This agrees with the behaviour of the simulated vehicle, which does not derail.

As for Nadal's index, it also remains quite below its limit value, leading to very similar results for both cases analysed.

Effect of embedded block spacing

Cases Analysed

In order to analyse the effect of embedded block spacing, the vehicle was simulated running on a curved track with the breakage located in the outer rail. As shown in Table 4, for a block spacing of 0.6, 0.8 and 1.0 m, three cases were considered for the stiffer embedded block system, Ms, (Mo, Mo-08 and Mo-06), and another three for the more elastic one, Ls, (Lo, Lo-08 and Lo-06).

Case	Block spacing [m]	Embedded block system (stiffness and damping)	Breakage location
Mo	1 m	KMS, dMS	Outer rail
Mo-08	0.8 m		
Mo-06	0.6 m		
Lo	1 m	KLS, dLS	
Lo-08	0.8 m		
Lo-06	0.6 m		

Table 4 Cases used to analyse the effect of embedded blocks spacing

Comparative results

In Figure 12 the results obtained are summarised.

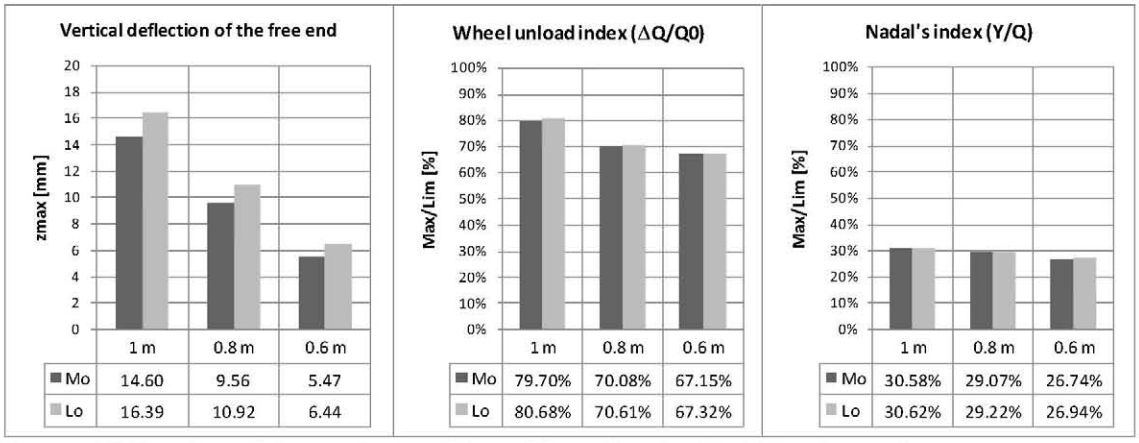

Figure 12 Results of the analysis of the effect of embedded block spacing

As can be seen, all the results remain below their corresponding limit value.

When comparing the derailment indexes, a great similarity between both embedded block systems can be seen. The difference is only slightly appreciable for the deflection of the free end of the broken track, which is greater for the more resilient system, Ls, as was expected.

In all cases, it can also be observed that the wheel unload index reaches higher values nearer to its limit value than in Nadal's index, which makes the former index more significant as a derailment criterion in this study.

As to the effect of embedded block spacing, it can be observed how its reduction also reduces the deflection of the free end of the broken track, as was expected, due to the corresponding length reduction of the cantilever section. This reduction is significant, with almost a 10 mm difference, when passing from 1 to 0.6 m spacing for both embedded block systems. In the same way, both derailment indexes decrease when reducing the embedded block spacing, with this effect being more appreciable for the wheel unload index by almost 10 %, and of little importance for Nadal's index.

Effect of the relative position of the rail breakage between two adjacent blocks

Cases Analysed

In order to analyse the influence of the relative position of the rail breakage between two adjacent blocks, two possible situations were considered: located in the furthest point from the first block (at the end of the block spacing), which is the reference position, and in the midpoint between two adjacent blocks.

The cases indicated in Table 5 were simulated, with the breakage located in the outer rail, and both at the end and the midpoint of the block spacing, for both embedded block systems, LS and MS.

Case	Breakage position	Embedded block system (stiffness and damping)	Breakage location
Mo	End	KMS, dMS	Outer rail
Mo'	Middle		
Lo	End	KLS, dLS	
Lo'	Middle		

Table 5 Cases used to analyse the effect of the relative position of the rail breakage between two adjacent blocks

Comparative results

The results obtained are summarised in Figure 13.

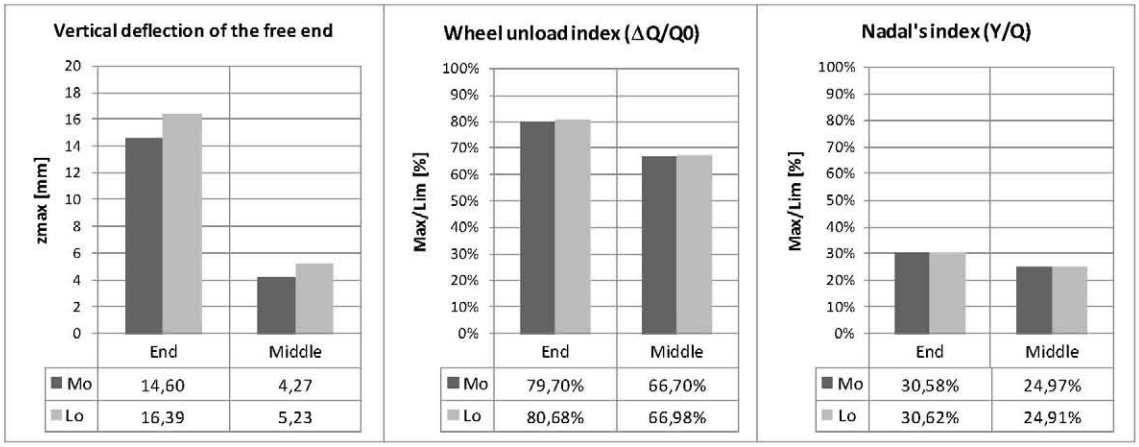

Figure 13 Results of the analysis of the effect of the relative position of the rail breakage between two adjacent blocks

As can be seen, all the results remain below their corresponding limit value.

As was expected, it was also observed that vehicle running safety is more unfavourable when the rail breakage is located in the furthest point from the first block. As before, the difference is more significant for the wheel unload index (13 %) than for Nadal's index (5 %), which remains quite distant from its limit value. This trend is more pronounced for the vertical deflection of the free end of the rail, with a difference greater than 10 mm between both situations.

According to these results, it was confirmed that locating the breakage at the end of the block spacing leads to a more unfavourable situation; therefore this location was chosen as the reference one for other comparisons.

Effect of the running speed

Cases Analysed

In order to analyse the effect of the running speed, several simulations were performed to assess the behaviour of the vehicle for speeds above and below the reference one, fixed at 80 km/h. Above 80 km/h, the speed was increased in 10 km/h intervals up to the derailment speed, which is 110 km/h. Below 80 km/h, speeds of 40 and 10 km/h were considered.

For all these speeds, the cases shown in Table 6 were simulated, with the breakage located in the outer rail and both embedded block systems, LS and MS.

Case	Speed [km/h]	Embedded block system (stiffness and damping)	Breakage location
Mo-110	110	KMS, dMS	Outer rail
Mo-100	100		
Mo-90	90		
Mo	80		
Mo-40	40		
Mo-10	10		
Lo-110	110	KLS, dLS	
Lo-100	100		
Lo-90	90		
Lo	80		
Lo-40	40		
Lo-10	10		

Table 6 Cases used to analyse the effect of the running speed

Comparative results

Figure 14 summarises the results obtained.

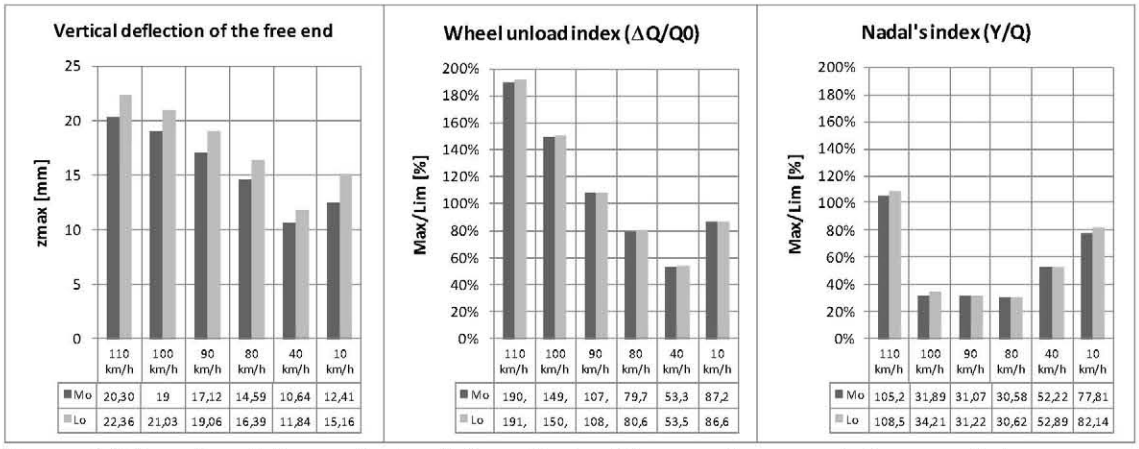

Figure 14 Results of the analysis of the effect of the running speed (bar graphs)

In order to better appreciate the differences between both embedded block systems, Ls and Ms, these results were represented again in the form of line graphs (Figure 15).

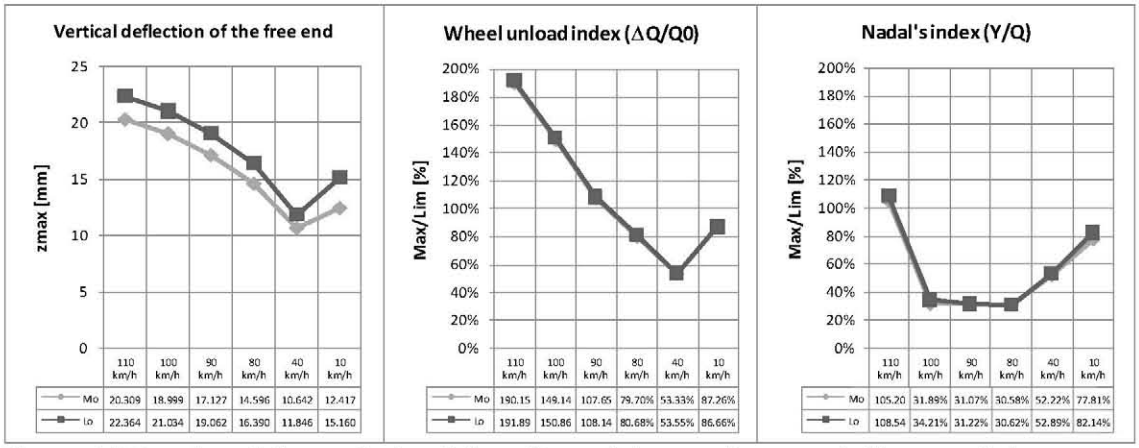

Figure 15 Results of the analysis of the effect of the running speed (line graphs)

As can be observed, increasing the speed from 80 km/h leads to more and more unfavourable safety situations. In particular, the deflection of the free end of the rail increases noticeably. With regard to the wheel unload index, this exceeds its limit value from 90 km/h, almost doubling it at 110 km/h. In spite of this, the vehicle only derails at 110 km/h, though not due to the rail breakage, but due to excess speed. As for Nadal's index, the increase observed by an increase in speed is much slighter, and only at 110 km/h does an appreciable increase occur, even when exceeding the limit value in this case, at which the vehicle actually derails, although outside the track section in which the breakage is located.

Reducing the speed from 80 km/h does not lead to more favourable safety situations. In particular, it was observed that very low speeds are more unfavourable than somewhat greater speeds. Thus, for 10 km/h, rail deflection is greater than for 40 km/h (and only slightly smaller than for 80 km/h). The wheel unload index is also greater for 10 km/h than for 40 and 80 km/h, reaching its minimum value at about 40 km/h. As for Nadal's index, a different trend is observed, since the reduction of the speed from 80 km/h causes a strong increase, reaching values close to its limit value for 10 km/h, although remaining below it.

The presence of a minimum value in the results could be justified considering that, when increasing the running speed on a curved track, the superposition of two antagonistic effects takes place. On the one hand, the time used to transmit the load from the wheels towards the rails is ever shorter, thus leading to decreasingly small deflections (see Figure 16). On the other hand, the centrifugal force in the vehicle is ever higher, so that the load transference towards the outer wheels is increasingly more significant, causing a greater deflection of the outer rail, in which the breakage is located.

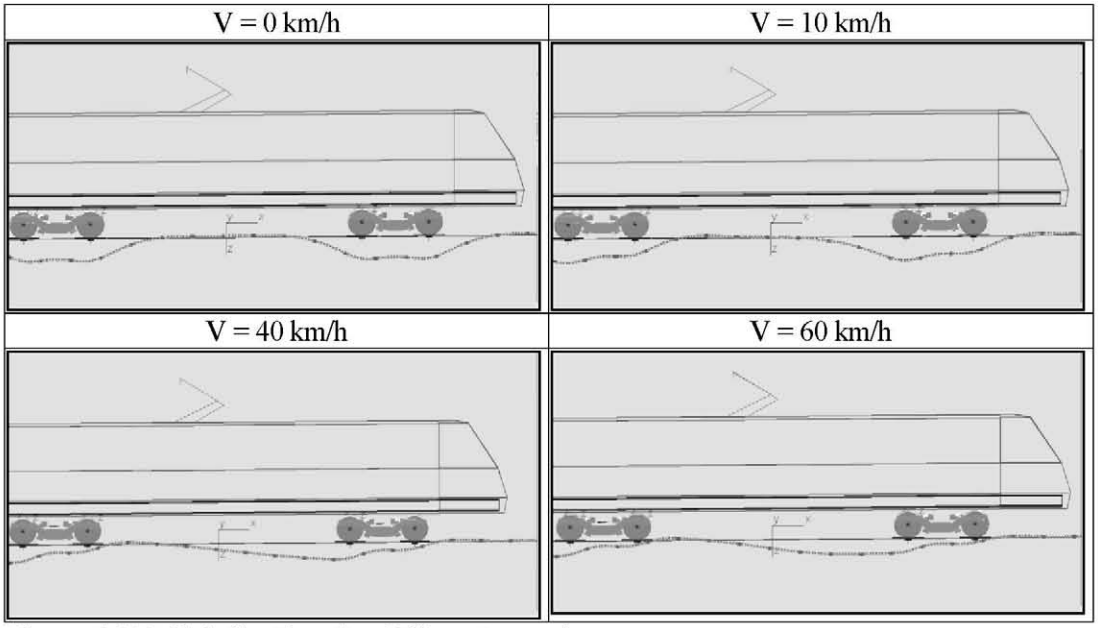

Figure 16 Rail deflection for different speeds

Concluding remarks

In this work, the running safety of metropolitan vehicles passing over a highly resilient curved slab track in the presence of a broken rail has been analysed, using combined MBS and FEM simulation techniques.

The effect of the rail on which the breakage is located, inner or outer, was analysed first. The effect of the embedded block spacing was also analysed, by reducing it from 1.0 m to 0.8 and 0.6 m. A more favourable location of the rail breakage than the reference one was also considered, going from a breakage located at the end of the block spacing to another located at the midpoint between adjacent blocks. All these situations were simulated for two elastic characteristics of the slab track fixation system, EBS MS and EBS LS, leading to the following conclusions:

- All the results obtained fall below the established limit values for both wheel unload and Nadal's indexes, and the vehicle did not derail in any of the cases analysed.
- For this study, the wheel unload index is more significant than Nadal's index, which remains quite below its limit value.
- With the exception of the values obtained for the deflection at the end of the broken rail, no significant differences were found from the safety point of view between the results obtained for the two embedded block systems analysed.
- The case with the rail breakage located in the outer rail of the curve is more unfavourable than the case with the rail breakage in the inner rail.
- The case with greater embedded block spacing is the most unfavourable one.
- The case with the rail breakage located at the end of the block spacing is more unfavourable than the case with the rail breakage at the midpoint between adjacent blocks.

Finally, the effect of the running speed on a curved track was also analysed, considering up to 8 different speeds, between 10 and 110 km/h, leading to the following conclusions:

- With the exception of the values obtained for the deflection at the end of the broken rail, no significant differences were found from the safety point of view between the results obtained for the two embedded block systems analysed.
- The deflection of the end of the broken rail reaches its maximum value for the unmoving vehicle. When increasing the speed from 10 to 110 km/h, the deflection diminishes up to 40 km/h, and then increases again. This trend, with a minimum value at about 40 km/h, could be justified considering the superposition of two antagonistic effects:
    - On the one hand, as the speed increases, the time used to transmit the load from the wheels towards the rails is ever shorter, thus leading to decreasingly small deflections.
    - On the other hand, the centrifugal force in the vehicle is ever higher, so that the load transference towards the outer wheels is increasingly more significant, causing a greater deflection of the outer rail, in which the breakage is located.
- Over 90 km/h, the limit value established for the wheel unload index is exceeded, while that for Nadal's index is only exceeded at 110 km/h, when the train derails due to excess speed, but not by any effect of the rail breakage.

According to the results obtained, it can be concluded that the use of the resilient fixations analysed does not noticeably affect vehicle safety if a rail breakage takes place on a curved track.

Acknowledgements

The authors gratefully acknowledge the kind help and advice of Alejandro Chércoles and Gabriel Banzo (Metro de Madrid) during the preparation of this research project. Special thanks go to Jenny Paulin (CITEF) for her contributions made throughout the whole process.

REFERENCES

1. **Gonzalez, F. J., et al.** Safety Assessment of Underground Vehicles Passing over Highly Resilient Straight Track in the Presence of a Broken Rail. *Journal of Rail and Rapad Transit.* 2008, Vol. 222, pp 69-84.
2. **Polach, O., Berg, M y Iwnicki, S.** Simulation. [aut. libro] S Iwnicki. *Handbook of Railway Vehicle Dynamics.* s.l. : CRC Press, 2006, pp 143-179.
3. **Dahlberg, T.** Track Issues. [aut. libro] S Iwnicki. *Handbook of Railway Vehicle Dynamics.* 143-179 : CRC Press, 2006.
4. **Esveld, C.** *Modern Railway Track.* s.l. : MRT-Productions, 2001. 90-800324-3-3.
5. *Modelling Dynamic Behaviour of Very High-Speed Railways to Evaluate Track Vibration and Deterioration.* **Afonso Ferreira, P. y López-Pita, A.** London, UK : s.n., 29-30 June, 2005. Railway Engineering - 2005.
6. **Frýba, L.** History of Winkler Foundation. *Vehicle System Dynamics Supplement.* 1995, Vol. 24, pp 7-12.
7. **Moravčík, M.** Response of Railway Track on Nonlinear Discrete Supports. *Vehicle System Dynamics Supplement.* 1995, Vol. 24, pp 280-293.
8. **Ahlbeck, D. R.** Effects of Track Dynamic Impedance on Vehicle-Track Interactions. *Vehicle System Dynamics Supplement.* 1995, Vol. 24, pp 58-71.
9. **Thompson, D. J. y Vincent, N.** Track Dynamic Behaviour at High Frequencies. Part 1: Theoretical Models and Laboratory Measurements. *Vehicle System Dynamics Supplement.* 1995, Vol. 24, pp 86-99.

10. **Jaschinski, A.** Multibody Simulation of Flexible Vehicles in Interaction with Flexible Guideways. *Vehicle System Dynamics Supplement.* 1995, Vol. 24, pp 31-44.
11. **Knothe, K., Wu, Y. y Gross-Thebing, A.** Simple, Semi-Analytical for Discrete-Continuous Railway Track and their Use for Time-Domain Solutions. *Vehicle System Dynamics Supplement.* 1995, Vol. 24, pp 340-352.
12. **Young, T. H. y Li, C. Y.** Vertical Vibration Analysis of Vehicle/Imperfect Track Systems. *Vehicle System Dynamics.* 2003, Vol. 40, pp 329-349.
13. **Ripke, B. y Knothe, K.** Simulation of High Frequency Vehicle-Track Interactions. *Vehicle System Dynamics Supplement.* 1995, Vol. 24, pp 72-85.
14. **Dahlberg, T.** Vertical Dynamic Train/Track Interaction – Verifying a Theoretical Model by Full Scale Experiments. *Vehicle System Dynamics Supplement.* 1995, Vol. 24, pp 45-57.
15. **Eisenmann, J.** Die Schiene als Tragbalken (The Rail as a Support Beam). *EI – Eisenbahningenieur.* 2004, Vol. 55, pp 22-25.
16. *Statistical Analysis of Rail Breakage and Rail Welding Failures in Iranian Railways.* **Zakeri, J. A.** London, UK : s.n., 29-30 June, 2005. Railway Engineering - 2005.
17. *Managing Risk on the Railway Infrastructure.* **Zarembski, A. M. y Palese, J. W.** Montreal, Canada : s.n., June 4-8, 2006. Proceedings of the 7th World Congress on Railway Research.
18. **Wu, T.X. y Thompson, D.J.** The Effects of Track Non-Linearity on Wheel/Rail Impact. *Journal of Rail and Rapid Transit.* 2004, Vol. 218, pp 1-15.
19. **Andersson, C. y Dahlberg, T.** Wheel/Rail Impacts at a Railway Turnout Crossing. *Journal of Rail and Rapid Transit.* 1998, Vol. 212, pp 123-134.
20. **Jeong, D. J.** *Engineering Study of Dynamic Loads at Rail Joints.* 2001.
21. **Dukkipati, R. V. y Dong, R.** The Dynamic Effects of Conventional Freight Car Running over a Dipped-joint. *Vehicle System Dynamics.* 1999, Vol. 31, pp 95-111.
22. *Super Resilient Rail Fixation Systems to Reduce Squeal Noise, Vibration and Rail Corrugation.* **Vanhonacker, P. y Van Leuven, A.** London, UK : s.n., 29-30 June, 2005. Railway Engineering - 2005.
23. *Achieving S3 or the Development of a Highly Resilient High-Speed Slab Track for the Channel Tunnel Rail Link.* **Bergoend, J. P., Petin, B. y Robertson, I.** London, UK : s.n., 29-30 June, 2005. Railway Engineering - 2005.
24. **Thompson, D. y Jones, C.** Noise and Vibration from Railway Vehicles. [aut. libro] S. Iwnicki. *Handbook of Railway Vehicle Dynamics.* s.l. : CRC Press, 2006, pp 279-325.
25. **Wu, H. y Wilson, N.** Huimin Wu and Nicholas Wilson. [aut. libro] S. Iwnicki. *Handbook of Railway Vehicle Dynamics.* s.l. : CRC Press, 2006.
26. *Circulación en Curva de Vehículos Ferroviarios.* **Giménez, José Germán.** Madrid : s.n., 2001. II Curso de Especialización en Tecnologías Ferroviarias.
27. **Melis, M.** Terraplenes y balasto en Alta Velocidad Ferroviaria (Primera parte). *Revista de Obras Públicas.* March 2006, 3464, pp 7-36.
28. **Melis, M. y González, F.J.** *Ferrocarriles Metropolitanos. Tranvías, Metros Ligeros y Metros Convencionales.* s.l. : Colegio de Ingenieros de Caminos, Canales y Puertos, 2004. 8438002870.

29. **Melis, M. y Matías, I.** Vía en Placa en la Ampliación del Metro de Madrid. Reducción de los Costes de Mantenimiento. *Revista de Obras Públicas.* April 1998, 3375, pp 17-34.
30. **Miura, S., y otros.** The Mechanism of Railway Tracks. [aut. libro] K. Wako. *Railway Technology Today 2.* s.l. : Japan Railway & Transport Review, March 1998, pp 38-45.
31. *Evaluating Track Structures: Life Cycle Cost Analysis as a Structured Approach.* **Zoeteman, A. y Esveld, C.** Tokyo : s.n., October 1999. World Congress on Railway Research.
32. **Man, A. y Hoogendoorn, C.** *Mechanical Test Results EBS Low Stiffness – Metro de Madrid.* EDILON Report R4293. January 2005.
33. **Houwen, G. y Wiltink, F.** *Mechanical Properties of the Metro de Madrid Medium Stiffness Embedded Block System.* EDILON Report R3713. March 2002.
34. **Edilon.** Edilon Corkelast® Embedded Block system. *Edilon Rail Systems.* [Online] [Cited: 19 November 2006.] http://www.edilon.com.
35. Sistema Bibloque sin Riostra. *Ingenieria de Vias Elasticas.* [Online] [Cited: 19 November 2006.] http://www.viaselasticas.com.
36. **Knothe, K. y Grassie, S.L.** Modelling of Railway Track and Vehicle/Track Interaction at High Frequencies. *Vehicle System Dynamics.* 1993, Vol. 22, pp 209-262.
37. **Schupp, G., Weidemann, C. y Mauer, L.** Modelling the Contact Between Wheel and Rail Within Multibody System Simulation. *Vehicle System Dynamics.* 2004, Vol. 41, pp 349-364.
38. *Models of Metro de Madrid Rolling Stock and Comparative Studies Relating the Comfort.* **Gonzalez, F.J., y otros.** Budapest, Hungary : s.n., 13-16 September, 2004. 6th International Conference on Railway Bogies and Running Gears.
39. **Miyamoto, M.** Mechanism of Derailment Phenomena of Railway Vehicles. *QR of RTRI.* 1996, Vol. 37, pp 147-155.
40. **Ishida, H. y Matsuo, M.** Safety Criteria for Evaluation of Railway Vehicle Derailment. *QR of RTRI.* 1999, Vol. 40, pp 18-25.
41. **UIC 518.** *Testing and approval of railway vehicles from the point of view of their dynamic behaviour - Safety - Track fatigue - Ride quality.* s.l. : Union Internationale des Chemins de Fer (UIC), 2005.
42. *Force-Based Assessment of Rail Welds.* **Esveld, C. y Steenbergen, M.** Montreal, Canada : s.n., June 4-8, 2006. Proceedings of the 7th World Congress on Railway Research.